1
2
3
Payload hardware and experimental protocol for testing the effect of space microgravity on the resistance to gentamicin of stationary-phase uropathogenic *Escherichia coli* and its σs-deficient mutant

4

5
AC Matin*, J-H Wang, Mimi Keyhan, Rachna Singh, Michael Benoit

6
Department of Microbiology & Immunology, Stanford School of Medicine,

7
Stanford, CA 94305, USA

8
9
10
11
12
Macarena P. Parra,* Michael R. Padgen, Antonio J. Ricco,* Matthew Chin, Charlie R. Friedericks, Tori N. Chinn, Aaron Cohen, Michael B. Henschke, Timothy V. Snyder, Matthew P. Lera, Shannon S. Ross, Christina M. Mayberry, Sungshin Choi, Diana T. Wu, Ming X. Tan, Travis D. Boone, Christopher C. Beasley, and Stevan M. Spremo

13
14
15
NASA Ames Research Center, Moffett Field, CA 94035, USA

16
*Corresponding author: a.matin@stanford.edu

17
*Other corresponding authors: macarena.p.parra@nasa.gov ,

18
antonio.j.ricco@nasa.gov

19

20

21

22

23

24

1

ABSTRACT

Human immune response is compromised and bacteria can become more antibiotic resistant in space microgravity (MG). We report that under low-shear modeled microgravity (LSMMG) stationary-phase uropathogenic *Escherichia coli* (UPEC) become more resistant to gentamicin (Gm). UPEC causes urinary tract infections (UTIs), reported to afflict astronauts; Gm is a standard treatment, so these findings could impact astronaut health. Because LSMMG has been shown to differ from MG, we report here preparations to examine UPEC's Gm sensitivity during spaceflight using the *E. coli Anti-Microbial Satellite* (*EcAMSat*) on a free-flying "nanosatellite" in low Earth orbit. Within *EcAMSat's* payload, a 48-microwell fluidic card contains and supports study of bacterial cultures at constant temperature; optical absorbance changes in cell suspensions are made at three wavelengths for each microwell and a fluid-delivery system provides growth medium and predefined Gm concentrations. Performance characterization is reported for spaceflight prototypes of this payload system. Using conventional microtiter plates, we show that Alamar Blue (AB) absorbance changes due to cellular metabolism accurately reflect *E. coli* viability changes: measuring AB absorbance onboard *EcAMSat* will enable telemetry of spaceflight data to Earth. Laboratory results using payload prototypes are consistent with wellplate and flask findings of differential sensitivity of UPEC and its Δ*rpoS* strain to Gm. Space MG studies using *EcAMSat* should clarify inconsistencies from previous space experiments on bacterial antibiotic sensitivity. Further, if σ^s plays the same role in space MG as in LSMMG and Earth gravity, *EcAMSat* results would facilitate utilizing our previously-developed terrestrial UTI countermeasures in astronauts.

48   **KEYWORDS**

49   Bacterial antibiotic resistance; microgravity; low-shear modeled microgravity

50   (LSMMG); stress response; sigma S; stationary phase; uropathogenic *E. coli*

51   (UPEC); *EcAMSat*; nanosatellite; cubesat; gentamicin; alamar blue; sigma-s

52   deletion.

53

54   **INTRODUCTION**

55   When *Escherichia coli* experiences stationary phase under Earth gravity, it induces the

56   general stress response (GSR), which makes it comprehensively resistant against a variety of

57   disinfectants.[1-4] GSR is controlled by the master regulator of this response, sigma S (σ^s, encoded

58   by the *rpoS* gene). This sigma factor controls the synthesis of a core set of proteins that protect

59   vital cell biomolecules, i.e., proteins, DNA, and the cell envelope.[3,4]

60   Like disinfectants, antibiotics cause cytotoxicity by damaging the biomolecules that the

61   σ^s-controlled proteins protect. We therefore recently tested the effect of the loss of this sigma

62   factor on the sensitivity of stationary-phase uropathogenic *E. coli* (UPEC) to the antibiotic,

63   gentamicin (Gm): the σ^s-deficient strain did indeed show enhanced sensitivity to the drug

64   relative to the unmodified strain.[5]

65   *E. coli* cultivated under what is often referred to as low-shear modeled microgravity

66   (LSMMG), generated by the use of high-aspect-ratio vessels (HARVs), also develop a σ^s-

67   dependent comprehensive resistance, which resembles GSR.[6] We note that the conditions in

3

68 HARVs are more precisely described as 'low-shear cell suspension', a term indicative of the

69 absence of gravitational cell sedimentation due to the flow of medium past the cells at low

70 interfacial shear rates. We will, however, continue to use the term LSMMG, which has been

71 widely adopted to describe such experiments. LSMMG-grown *E. coli* become more resistant to

72 high salt, low pH, and ethanol[5-7] and, as we show here for UPEC, also to Gm.

73 UPEC is a causative agent of urinary tract infection (UTI), for which Gm is standard

74 treatment. UTI has been reported in astronauts.[8] Therefore, if the LSMMG findings are

75 applicable to actual microgravity of space (MG), they would indicate a potential threat to space

76 travelers, especially since there is growing evidence that the human immune response is

77 weakened by MG.[9-11] However, LSMMG may not have full fidelity to space MG, and it is thus

78 necessary to examine Gm sensitivity of UPEC in *in-situ* space experiments.

79 Biological experiments on the Space Shuttle and the International Space Station (ISS) can

80 be limited and costly because of crewmember involvement and other factors. NASA has

81 therefore developed fully autonomous microsystems in the form of free flying "nanosatellites"

82 for space experimentation. Examples are: *GeneSat*, *PharmaSat*, and *O/OREOS*.[12-15] These

83 platforms avoid astronaut involvement and permit experimentation in more orbital locations than

84 ISS. *PharmaSat* has been used to measure the effects of low-Earth-orbit microgravity ($< 10^{-3}$ x

85 Earth gravity) on the sensitivity of the yeast *Saccharomyces cerevisiae* to the antifungal agent

86 voriconazole.[13,14] We have modified *PharmaSat* for experiments with bacteria in order to

87 determine *E. coli* sensitivity in space to Gm. The modified payload system (referred to as

88 *EcAMSat*, short for *E. coli* Antimicrobial Satellite) and tests of its suitability for space

89 experiments are described here.

90 Given the findings of Wang et al.[5] under Earth gravity of the involvement of σ^s in Gm

4

91 resistance, we have included in these studies the Δ*rpoS* mutant of UPEC, missing σ^s. Should it

92 turn out that the enhanced resistance of UPEC to Gm in MG also depends on this sigma factor, it

93 would indicate new ways of controlling UPEC resistance to Gm during space flight.

94 We have focused on stationary-phase bacteria in this and our previous studies[4,5,16] for the

95 following reasons: a) bacteria in this phase are hard to eradicate; b) due, for example, to lack of

96 nutrient or the presence of oxidative stress, this late-growth phase is often experienced by

97 bacteria in the human host;[1-3,17] and c) stationary-phase bacteria express virulence traits required

98 for disease causation;[18-24] an example is UPEC Type I fimbriae, which it uses in bladder

99 colonization.[25, 26]

MATERIALS AND METHODS

101 **LSMMG effect on Gm sensitivity.** To determine the effects of cultivation under

102 LSMMG on Gm sensitivity, the wild type and the Δ*rpoS* UPEC strains were cultivated in HARV

103 reactors as described previously.[6] Pairs of the reactors were rotated about appropriate axes:

104 vertical for normal gravity ('HARV NG') and horizontal for LSMMG conditions. 50 mL of

105 Luria broth (LB) medium was used in each vessel. Overnight conventional-flask LB cultures

106 were used as inoculum; the starting absorbance at 660 nm (A_{660}) was 0.1, and the HARVs were

107 rotated at 25 revolutions per minute. Following 24-h incubation (37 °C), the stationary-phase

108 cells were harvested from the HARVs, re-suspended in M9 salts (referred to from hereon as

109 'M9') to an A_{660} of 0.4, and mixed with sufficient Gm to give a final concentration of 16 µg/mL.

110 After 24-h incubation (37 °C) under static conditions, viability was determined by counting

111 colony-forming units (CFU) using LB plates.

112 **Determination of the suitability of Alamar Blue to assess Gm effect on UPEC**

113 **viability.** To test the effect of space MG in inflight experiments, a method for UPEC viability

114 assessment is needed, the results of which can be transmitted from space to Earth via telemetry.

115 The dye Alamar Blue (AB) was used as a reporter for this purpose in the *PharmaSat* mission

116 concerning yeast viability mentioned above.[14] The yeast cell metabolic activity resulted in AB

117 reduction, causing its color to change from dark blue to magenta, thus increasing absorption at

118 525 and decreasing it at 615 nm; from this conversion the relative change in cell viability could

119 be assessed.[12] Concomitant measurement at 470 nm, where absorbance is weak for both reduced

120 and oxidized forms of AB, indicated solution turbidity and thus cell population.

121   Measured absorbance at 615, 525, and 470 nm only approximates the respective amounts

122 of oxidized AB, reduced AB, and cell-related turbidity. To more accurately determine these

123 parameters, we measured complete visible absorbance spectra of oxidized AB, reduced AB, and

124 a suspension of *E. coli*. We then used the absorbance values at the three measurement

125 wavelengths to calculate "cross terms" that correct for the fact that the absorbance spectrum of

126 (blue) oxidized AB has a shoulder at 525 nm and a tail at 470 nm, that the spectrum of (magenta)

127 reduced AB also has a tail at 470 nm, and that light scattering by the bacteria occurs throughout

128 the visible range, varying with a weak linear wavelength dependence. All graphics and results

129 reported below for quantities of oxidized AB, reduced AB, and cell turbidity have been corrected

130 accordingly.

131   To determine if the AB-conversion method can be used for assessing UPEC viability, the

132 wild type and its isogenic Δ*rpoS* mutant[5] were grown in conventional laboratory flasks shaken

133 overnight at 200 rpm in 1/6-strength LB at 37 °C. As before,[16] growth under these conditions

134 was complete within 6 hours, allowing some 8 hours of starvation in stationary phase; this

135 starvation period permits activation of GSR in the wild type.[27] The cultures were then diluted to

136 an A_{600} of 0.45 in M9. Gm (Sigma-Aldrich, St. Louis, MO) was added to both the wild type and

137   the mutant cultures to a final concentration of 16 µg/mL; a parallel aliquot of cell suspension of

138   each strain without the drug served as control. Following 24-h incubation without shaking, 1.8

139   mL of the cultures were transferred to test tubes to which 200 µL of 10x AB (ThermoFisher

140   Scientific, Grand Island, NY) was added. To monitor changes in AB absorption, the cultures

141   were dispensed in microtiter plate wells (Figure 3B; Thermo Scientific, Waltham, MA), each

142   well receiving 0.25 mL. Appropriate control solutions in other rows of the well plates were also

143   in 0.25 mL quantities, and five wells were used for each condition. Absorption changes at 470,

144   525, and 615 nm were measured in a microplate reader (Biochrom US, Holliston, MA); data

145   were acquired by DigiRead software (ASYS Hitech, Holliston, MA) and transferred to Excel

146   (Microsoft, Redmond, WA) for analysis.

147   *EcAMSat* **payload system.** In this system, the *E. coli* cells are placed in the payload

148   hardware in a 48-well fluidic card (Figure 1; Micronics, Redmond, WA). The cards are made

149   from laser-cut layers of poly(methylmethacrylate) bonded together with pressure-sensitive

150   acrylic adhesive (9471LE on 51-µm-thick Melinex 455 polyester carrier, 3M; St. Paul, MN).

151   Each well (4.0 mm diameter x 7.8 mm long; 100 µL volume) is fitted at its inlet and outlet with

152   0.2-µm filters (nylon fiber; Sterlitech, Kent, WA) to prevent cell leakage. Well tops and bottoms

153   are sealed by 50-µm-thick air-and-CO_2-permeable optical-quality poly(styrene) membranes.

154   Attached to both sides of the card are thermal spreaders (thin aluminum plates), each containing

155   three embedded AD590 temperature sensors that provide output current directly proportional to

156   absolute temperature (Analog Devices, Norwood, MA); a thin-film heater fabricated from kapton

157   tape and patterned metal conductors (Minco, Minneapolis, MN) is affixed to the opposite side of

158   each spreader plate, relative to the fluidic card, and controlled in a closed-loop fashion using the

159   temperature sensor outputs.   Each well is equipped with its own 3-color LED (LTST-

160 C17FB1WT; Lite-On Technology Corp., Taiwan); a photodetector (Model no. TSL237T; AMS-

161 TAOS USA, Plano, TX) at the opposite end of each well converts the transmitted light intensity

162 to a proportional frequency, from which absorbance values can be calculated. (No moving parts

163 are associated with the optical measurements.) The card, thermal spreaders, and printed-circuit

164 (PC) boards supporting the LEDs and photodetectors, which are placed on opposite sides of the

165 fluidic card, constitute the "card stack" (see the cross section, upper right in Figure 1).

166   The card fluid-delivery system (Figure 1) includes 11 electrically-actuated solenoid

167 valves (SVs, LHDA0531315HA; The Lee Co., Westbrook, CT); a diaphragm pump for high-

168 flow-rate fluid mixing, circulation, and priming of tubing (NF 5S; KNF Neuberger, Trenton, NJ);

169 a precision metering pump (LPVX0502600BC; The Lee Co.) to prepare and deliver the desired

170 concentrations and volumes of antibiotic and other reagents; three 35-mL and six 25-mL reagent

171 bags (fluorinated ethylene propylene, FEP; American Fluoroseal/Saint-Gobain, Gaithersburg,

172 MD); a bubble trap (custom fabricated by NASA Ames); and a check valve (Smart Products;

173 Morgan Hill, CA) to prevent waste fluids from flowing back into the system. The 48 wells are

174 configured in 4 fluidically independent rows or "banks" of 12 each (labeled "High", "Medium",

175 "Low", and "Control" in Figure 1, indicating the relative Gm concentrations that were

176 administered). Each bank on the inlet side of the card is connected to the normally-closed port of

177 one SV and, on the outlet side, to a 25-mL waste bag partially filled with M9 salts (without

178 glucose; Sigma-Aldrich, St. Louis, MO; referred to from hereon as 'M9'); pressurization (~7

179 kPa) of these waste bags by means of a spring-loaded metal plate replaces any fluid that

180 evaporates over time from the wells through their permeable membrane cover. The nutrient

181 (1/6-strength LB), antibiotic (Gm), antibiotic dilution medium (M9), and AB bags are also

182 attached to SV NC ports (Figure 1). A Gm-dilution loop is created by attaching the M9 bag via

183 another SV near the outlet of the bubble trap, which is placed ahead of the point of fluid delivery

184 to the card. The main waste bag collects the previous contents of the tubing each time it is filled

185 with a new reagent (see below) prior to delivery to the card.

186   Figures 2A and 2B show, respectively, the assembled *EcAMSat* payload fluidic system

187 hardware and the hermetically sealed containment vessel (internal volume ~ 1.2 L) in which the

188 system is housed. The sealed payload containment vessel is integrated with the spacecraft "bus",

189 which includes the power, communications, data-handling, and control functions. The completed

190 nanosatellite has overall dimensions of 10 x 22 x 36 cm.

191   **AB-mediated assessment of Gm effect in the *EcAMSat* payload on Earth.** The wild

192 type and $\Delta rpoS$ mutant of UPEC were grown as described above, rinsed with M9 (3x), and

193 diluted in M9 to an A_{600} of 1.0. In a sterile biosafety cabinet, 5 μL aliquots of each strain were

194 loaded in alternating wells of the 48-well fluidic card so that six of the 12 wells per bank

195 contained the wild type and six the mutant. The card was sealed and purged with CO_2 to

196 facilitate bubble-free filling of the channels and wells: any CO_2 bubbles remaining after priming

197 with degassed M9 dissolved readily as additional M9 flowed through the wells. The card was

198 manually primed with a syringe containing degassed M9 connected to the outlet, and a second

199 empty syringe at the inlet, its plunger drawn back to generate a slight vacuum. After filling and

200 until connection to the fluidic system, the card remained under pressure (~4.4 kPa) from a bag of

201 M9 hanging approximately 45 cm above the card; this served to replace any fluid lost by

202 evaporation through the permeable membranes and thereby prevented bubble formation in the

203 wells. The rest of the sterile fluidic system was filled with the appropriate solutions (see Figure

204 1), assembled with the rest of the payload hardware, and then sealed in the hermetic containment

205 vessel; as explained above, slightly pressurized M9 in the waste bags continued to compensate

206   for any evaporation. As placement in the containment vessel eliminated further need for a sterile

207   environment, the assembled payload system was removed from the biosafety cabinet and

208   attached to a benchtop "rotisserie" apparatus; this rotated the payload first clockwise and then

209   counterclockwise by nearly one full rotation with a period of ~ 80 s, preventing cell settling. The

210   experiments were run using ground-support equipment, i.e., a desktop computer and power

211   supply, and employed a "space-flight-like" command sequence.

212   To start the viability measurements, the 3-color LEDs with emissions at the above-

213   mentioned wavelengths were sequentially energized, one color and one well at a time. The

214   photodetector of each well converted the transmitted light intensity of each color to a

215   proportional frequency, permitting calculation of absorbance. (During the spaceflight

216   experiments, the stored frequencies will be telemetrically transferred to Earth from the satellite.)

217   The measurements for each well were taken every 15 min. The payload system was warmed to

218   37 °C for ~3 hours (Figure 2C) by the heaters and thermal spreaders with closed-loop

219   temperature control using the mean value from the six temperature sensors. 1/6-strength LB was

220   pumped into each bank in turn, starting with the control bank, replacing the M9. The pumping

221   phase lasted for two hours per bank (see Results section for total durations of the various

222   phases). The cells were allowed to grow to stationary phase and then to starve. Next, the

223   metering pump delivered M9 to the control bank; each well received ~ 4x its 100 µL volume to

224   reach at least 90% exchange. The metering pump then extracted a small, measured amount of

225   concentrated Gm from the antibiotic bag and delivered it to the M9 dilution bag (Figure 1); the

226   Gm-dilution loop was opened and the diaphragm pump operated to mix the antibiotic and M9.

227   After delivery of the resultant lowest concentration of Gm to the Low bank (~4x exchange), the

228   process was repeated to deliver the medium and high Gm concentrations to the Medium and

229   High banks, respectively. Following incubation with Gm, AB was added, displacing the M9 in

230   the Control bank and the Gm in the other banks.

231   **Determination of 'stasis' effect.** An approximately six-week delay is expected between

232   loading of cells and reagents into the satellite hardware and initiation of the experiments in

233   space. To determine the effect of such stasis on cell viability, Gm strength, and AB properties,

234   the cells were incubated without shaking in M9 for 10 weeks and the reagents were stored for

235   this duration in the same types of bags that will be used for the space mission. Cell viability was

236   determined by cell count; the Gm and AB activities were assessed by comparing the effect of

237   aged reagents with fresh ones in cell killing and assessing cell activity, respectively.

238

239   **RESULTS**

240   **LSMMG cultivation makes UPEC more resistant to Gm but not its Δ*rpoS* mutant.**

241   We examined the effect of LSMMG cultivation on Gm sensitivity of UPEC: cells were

242   cultivated in HARV reactors to stationary phase and then exposed to Gm for 24 h. LSMMG-

243   grown UPEC was significantly more resistant to Gm than the control culture grown under

244   HARV NG conditions ($29 \pm 2\%$ vs. $18.6 \pm 1.2\%$ survival, $p < 0.01$). This is reminiscent of the

245   well-established effect of LSMMG on enhanced resistance of *E. coli* to disinfectant agents.[6,8]

246   Consistent with results with cells grown under NG in conventional flasks,[5] the Δ*rpoS* mutant was

247   more sensitive to the drug than the wild type also under the HARV NG conditions ($2.33 \pm 0.09\%$

248   vs. $18.6 \pm 1.2\%$ survival, $p < 0.01$). Furthermore, as in the case of disinfectant agents, the

249   mutant, unlike the wild type, failed to show increased Gm resistance under LSMMG; indeed,

250 under these conditions, it was more sensitive than its HARV NG-grown counterpart (0.21 ±

251 0.07% vs 2.33 ± 0.09% survival, $p < 0.001$).

252 Thus, LSMMG stress makes *E. coli* comprehensively resistant, including to an important

253 drug, and this effect is σ^s-dependent. LSMMG may not fully represent space MG conditions, but

254 given its relevance to these conditions, this finding constitutes a potential threat to astronaut

255 health. This warrants corroboration under actual space MG to determine if countermeasures must

256 be devised to safeguard astronaut health. Towards this end, the following experiments were

257 carried out using the *EcAMSat* payload platform described in Materials and Methods.

258 **Alamar Blue absorption changes permit determination of UPEC viability.** As stated

259 above (Materials and Methods), we tested AB as reporter for assessing cell viability to transmit

260 results of the planned space experiments to Earth. For these experiments, our previous

261 experimental protocol was used.[5] This entailed the following phases: growth, followed by

262 starvation (needed to activate GSR), Gm treatment, and viability determination by CFU counts;

263 in the present case, we substituted AB absorbance changes for the colony counting. The growth

264 and starvation phases lasted 12 hours each, Gm treatment, 24 hours, and AB assessment of

265 viability, 6 hours.

266 The results of the CFU counts of our previous work are reproduced in Figure 3A for

267 convenience of reference;[5] they show that, compared to the wild type, Gm treatment causes a

268 greater loss of viability in the UPEC strain missing the *rpoS* gene. Figure 3B shows the color

269 changes of Alamar Blue in 96-well plates due to the metabolism of the treated and untreated wild

270 type and Δ*rpoS* mutant strains (the rows of wells are aligned to the bars of Figure 3A

271 representing the colony counts): it is clear that the AB absorption changes correlate well with the

272 CFU counts.

273   Using a conventional well-plate reader, absorbance at 470, 525, and 615 nm was

274   measured and used as described above to calculate the relative concentrations of the oxidized and

275   reduced forms of AB and the optical density (turbidity) at the indicated time points. Figures 3C-F

276   show these results when AB was used to assess the effect of Gm on the viability of the two

277   strains; the controls (M9 alone and M9 + AB; data not shown in the figure) showed no change in

278   absorbance. As indicated by lack of change in cell turbidity (black and grey curves; Figures 3C,

279   D), no growth occurred during these experiments under any of the conditions.   Pairwise

280   comparisons, for the two strains, of the loss of blue AB or appearance of magenta AB with and

281   without Gm (Figures 3C and 3D, respectively) yield $p < 0.0001$ in all four cases.

282   The concentrations of the blue (oxidized) form of AB for each strain and each condition

283   are plotted vs. time in Figure 3E, which shows clearly that the amount of AB reduced by both

284   strains when treated with Gm is less than for the respective untreated controls.   Figure 3F

285   compares the relative magnitude of the effect of the antibiotic on the wild type and mutant using

286   the $t = 6$ hour results from Figure 3E. The heights of the bars are the percentages of AB reduced

287   in the presence of Gm divided by the amount of AB reduced in the absence of Gm, for each

288   strain. The results show that the Gm-treated wild type, which reduced $74.4 \pm 2.2\%$ of the amount

289   of AB reduced by untreated wild type, differs significantly from Gm-treated mutant, which

290   reduced $60.5 \pm 3.2\%$ of the amount of AB reduced by untreated mutant ($p < 0.001$). Thus, in

291   both strains changes in AB absorption resulting from metabolic activity agree qualitatively with

292   the Gm effect found by CFU measurements.

293   **The *EcAMSat* system permits efficient dilution and exchange.** It is of course essential

294   that the dilutions and exchanges needed to conduct the experiments in the *EcAMSat* hardware be

295   accurately accomplished.   Antibiotic is carried in the payload in a concentrated form (400

296 μg/mL) and will require dilution to the planned three specific concentrations at the time of the

297 space experiment. To determine antibiotic dilution accuracy, a 1% solution of non-toxic yellow

298 dye (absorbance maximum ~ 414 nm) in M9 was loaded into the antibiotic bag in place of Gm

299 (see Figure 2). The payload was assembled but not loaded into the hermetic containment vessel

300 so that the system was in near-flight-like configuration but with the tubing accessible during

301 pumping. Samples were obtained during pumping of the dye. The absorbance of each sample,

302 diluted using the *EcAMSat* payload system, was measured at 414 nm, and the equivalent Gm

303 dose was calculated using a standard curve. The accuracy of this dilution process was measured

304 for three different "builds" of the fluidic system (i.e., different fluidic cards, sets of tubing,

305 pumps, valves, etc.). Figure 4A shows measured dilutions using dye that correspond to Gm doses

306 of 3.5, 14.6, and 52 μg/mL, corresponding to a systematic error of 9 – 16% below the intended

307 concentrations; the coefficients of variance are 4 – 5% for the medium at high concentrations and

308 20% for the low; the latter is not unexpected due to its high dilution ratio. Because of the

309 reasonably low degree of the deviations from the specified concentrations, and the fact that they

310 will occur in both the spaceflight and ground control systems, they are not expected to

311 significantly impact the results.

312   Fluid exchange in the banks is required to make transitions from initial stasis buffer to the

313 following phases: feeding-and-starvation; Gm dosing; and finally AB-mediated viability

314 measurement. To quantify the extent and consistency of these exchanges, 0.2% blue food dye in

315 M9 was loaded in the AB bag and pumped into all four banks of the card using the same flow

316 rate and duration as for the planned exchanges in the actual experiments (~4x volume exchange).

317 The payload was then disassembled, and the absorbance of the dye at 620 nm was measured in

318 the wells, using a well-plate reader. To ascertain the extent to which the replacement of M9 by

319   the dye was less than 100%, the dye was introduced into the banks under pressure (4.4 kPa) to

320   saturate the wells with it. The dye-filled bag was hung ~45 cm above the card and 6 mL of the

321   dye was allowed to flow through each bank (~1.5 mL volume): subsequent measurement

322   provided absorbance of the wells at 100% exchange. Background absorbance was determined

323   following flushing the card with M9 (which has zero absorbance at 615 nm). The background

324   was subtracted from both of the above measurements, and the absorbance of the blue dye

325   following pumping as a percentage of the absorbance at 100% exchange was calculated. Figure

326   4B shows that, with some bank-to-bank and test-to-test variability, the exchange efficiency in the

327   wells overall was near, and often greater, than 90%.

328   ***EcAMSat* payload exerts additional stress, but can reproduce the *rpoS*-dependent**

329   **UPEC resistance to Gm.** We next determined if the AB method can be used to assess Gm's

330   effect on the two UPEC strains in the *EcAMSat* payload system, using absorbance changes at the

331   same three wavelengths as the well-plate measurements and converting absorbance as described

332   above to quantities of oxidized and reduced AB (Figure 5A). The environment provided by this

333   system for the cells is closed and exposes them to its potentially stressful constituents, such as

334   poly(methylmethacrylate), the acrylic-based pressure-sensitive adhesive, and poly(styrene); it

335   was therefore not surprising that cells in this setup grew more slowly: some 20 hours were

336   required for growth completion (Figure 5B), as opposed to six hours in conventional flasks

337   (Materials and Methods). Given this relative sluggishness, we extended the starvation, Gm-

338   treatment, and AB-viability phases of the experiments to 30, 45, and 50 hours, respectively (see

339   Figure 5A).

340   The reduction of AB by wild type and mutant strains, both untreated and gentamicin-

341   treated (52 µg/mL), is shown in Figures 6A and 6B, respectively. As in the well-plate

342   experiments, no change in the cell-related turbidity occurred during the experiment for either

343   strain, indicating absence of growth (Figure 6A, B: black and gray curves). There was a more

344   marked difference in the metabolic activity of the untreated wild type and the mutant strains

345   (Figure 6A) in the payload setup than was seen in the microplate experiments (Figure 3C). Given

346   that the payload environment is stressful and absence of the *rpoS* gene broadly weakens UPEC,[4]

347   this was expected and necessitated, as in the well-plate experiments, normalization of the effect

348   of Gm on the two strains to take into account this baseline difference.

349   Figure 6C shows the (un-normalized) relative concentration vs. time of the oxidized form

350   of AB for both the wild type (black/grey curves) and mutant (green curves) strains for all Gm

351   doses: control, low (3.5 µg/mL), medium (14.6 µg/mL), and high (52 µg/mL). As with the well-

352   plate experiment, a meaningful comparison of the relative activity of Gm-treated wild type and

353   mutant strains required normalization for their respective untreated levels of activity. This was

354   done as described above (Figure 6D). To enable comparison with the well-plate experiments, we

355   chose for the results shown in Figure 6D the time point at which the Gm-treated wild type

356   control had reduced 74% of the AB ($t = 11.5$ hour: see vertical red line, Figure 6C), analogous to

357   the final time point of the well-plate experiment, at which 74% of the AB had also been reduced

358   ($t = 6$ hour in Figure 3D, E, from which Figure 3F data were obtained). While this comparison

359   reveals little difference between the effects of Gm on the two strains at the lower doses (Figure

360   6D), there is a significantly larger effect on the mutant relative to the wild type at the high dose

361   of Gm (52 µg/mL): wild type, $74.5 \pm 0.5\%$ of untreated change; mutant, $64.1 \pm 2.2\%$ of untreated

362   change; $p < 0.001$. This result is comparable to the well-plate result, albeit at a higher Gm dose.

363   The reason why the mutant exhibits differential sensitivity only at higher drug concentration is

364   not clear and would require further work to disentangle the interaction between the stresses of

365   the payload system and that exerted by Gm. Nevertheless, it is clear that the system designed

366   here is capable of answering the basic queries of interest, namely, would space MG increase Gm

367   resistance of UPEC and would it do so in an *rpoS*-dependent manner?

368   **Determination of bacterial viability and reagent strength with 'aging' during the**

369   **stasis period.** For our upcoming *EcAMSat* spaceflight experiment, there is some uncertainty

370   concerning the interval of time that will elapse between the loading and integration of all payload

371   constituents, including the bacteria in stasis, and the start of the experiment onboard the

372   nanosatellite in a stable Earth orbit: it could exceed six weeks. Accordingly, we determined the

373   effect of such a stasis period on bacterial viability and reagent strength; based on experience with

374   *PharmaSat*, tests were conducted for a stasis period of ca. 10 weeks. Consistent with previous

375   studies,[5] the Δ*rpoS* mutant retained less viability compared to the wild type: 0.3 vs. 0.7%. Gm

376   was found to lose some 50% of its potency. These differences will be compensated for by

377   appropriately adjusting the loading concentrations. AB and LB did not change their potency

378   during this period.

379

380   **DISCUSSION**

381   Concern about human health during space travel has been of central interest since the

382   inclusion of humans in space flights. Chief among these have been issues such as the effects of

383   microgravity on bone density, muscle strength, and cardiac function; to these, more recently have

384   been added the potential dangers of greater susceptibility of humans to infectious disease.[28,29]

385   There is compelling evidence that human immune response is compromised in space

386   flight.[28] Thus, after space flight, the oxidative burst capacity of monocytes and neutrophils of

387 astronauts is diminished, as are the functions of their natural killer and T cells; cytokine

388 production patterns are altered, likely accounting for the reactivation of herpesviruses seen in

389 astronauts; stress hormones are increased; and there is a tendency to shift to the Th2 pattern

390 (cytokine secretion resembling that of Th2 lymphocytes). Exposure to hypoxia or hyperoxia

391 within the spacecraft or during spacewalks can further weaken the immune response.[11,30-32]

392   This danger is compounded by the possibility that bacteria become more virulent in

393 microgravity. Wilson *et al*.[33] showed that, following culture on the Space Shuttle, *S.*

394 *Typhimurium* became more virulent in mice. Furthermore, the bulk of evidence, gathered in

395 LSMMG studies, indicates that bacteria may become more resistant in MG to disinfectant

396 agents, such as high salt and ethanol[8] and, as we show here, including an important antibiotic.

397   Bacterial antibiotic resistance has been examined also in actual MG during space flights,

398 but the results have been contradictory. Thus, while cultivation onboard Salyut 7 resulted in an

399 increase in the minimum inhibitory concentration (MIC) of *E. coli* to colistin and kanamycin,[34]

400 studies on the Space Station MIR indicated mostly decreased MIC to several antibiotics.[35] These

401 pioneering studies indicating at least the possibility of increased bacterial drug resistance in

402 space require further in-depth examination. It is towards this end that we have developed and

403 tested the payload system described here. We demonstrate that our microfluidic cards and fluid

404 delivery systems, along with the capability of AB to indicate *E. coli* viability, can be effectively

405 used with space experimentation hardware and protocols. In combination with the advantages

406 conferred by the use of nanosatellite systems, this platform provides an excellent approach for an

407 in-depth study of bacterial drug resistance during space flight.

408   The dependence on σ^s of LSMMG-conferred heightened resistance of UPEC to Gm that

409 we show here is akin to the role of this sigma factor in this resistance seen under Earth gravity.[5]

410   The latter studies identified several proteins of the antioxidant defense of this bacterium that can

411   be targeted to enhance the efficacy of this drug. Examples span reactive-oxygen-species (ROS)

412   quencher proteins (e.g., superoxide dismutase and catalase); and those of the pentose phosphate

413   pathway that supply the NADPH that the quencher proteins require for their activity (e.g.,

414   glucose-6-phosphate, the phosphogluconate dehydrogenases, and transaldolase A). We are at

415   present screening small compound libraries for inhibiting these proteins that could conceivably

416   be used in synergy with Gm to enhance its efficacy. If the space experiment corroborates the

417   LSMMG effect of σ^s-dependence of Gm resistance, such inhibitor compounds could prove

418   valuable in combating UTI in astronauts during space travel. Also, the behavior of the $\Delta rpoS$

419   mutant in inflight experiments will critically test whether the findings of the LSMMG studies,

420   namely that *E. coli* perceives MG as a stress, are accurate.

421   Like the effect of space MG on drug resistance, other aspects of microbial biology have

422   been reported to be affected differently by this gravity condition in different studies. In several

423   experiments on US Space Shuttle missions, Klaus *et al*. reported a shorter lag phase and a longer

424   exponential phase compared to ground controls,[36] ascribing this effect to the formation of a

425   'pseudo-membrane' in the form of an osmotic solute gradient interfering with nutrient flux to the

426   cells. However, it has been reported[37,38] that spaceflight affected neither the lag nor the

427   exponential phase in *E. coli*. Our planned spaceflight experiments promise to shed light on these

428   questions as well.

429

Legends

Figure 1. Schematic diagram of *EcAMSat* fluidic system (at left) connected to *EcAMSat* 48-well fluidic card (at lower right). A single fluidic well is also shown in cross section (top right). SV = 3-way solenoid valve; green arrows show direction of fluid flow; Waste H, M, L, C collect the flow-through from the High, Medium, Low, and Control banks of 12 wells each; other components are as marked.

Figure 2. **A)** Fully assembled *EcAMSat* biological/fluidic/optical/thermal payload system; **B)** its hermetic payload containment vessel with electrical interface board; overall size ~ 10 x 10 x 20 cm. **C)** Chronological summary of the sequence of operations and measurements for the ground experiments conducted to date; the spaceflight system will follow the same timeline.

Figure 3. **A**) Counts of colony-forming units for wild type (WT) and Δ*rpoS* mutant strains of *E. coli* without and with gentamicin ("Gm") treatment at 16 μg/mL (reproduced from ref. 39 for convenience of references). **B**) Color changes of Alamar Blue in 96-well plates due to metabolism of treated and untreated WT and Δ*rpoS* mutant; well rows are aligned to corresponding bars of Panel A; control row ("AB + M9") shows initial, unchanged blue color of AB in the absence of cellular metabolism. **C**) Time dependence of relative concentrations of oxidized (blue/turquoise curves) and reduced (pink/magenta curves) forms of AB along with OD (turbidity; black/grey curves) due to wild type ("WT") and mutant ("Mut") cells in absence of Gm measured with a wellplate reader. **D**) Same measurement as in Panel C but in the presence of 16 μg/mL Gm. **E**) Time dependence of concentration of blue (oxidized) AB for each strain (WT in black/grey; mutant in green/light green) without and with Gm treatment. **F**) Relative magnitude of the effect of Gm on the two strains based on the t = 6-hour data from Panel E; each

454   bar is normalized to the amount of AB reduction measured for the respective strain in absence of

455   Gm treatment ($n = 6$; $p < 0.0001$). Error bars in Panels C through F are ± one standard deviation.

456   **Figure 4. A**) Expected (calculated) and optically measured (using dye) equivalent doses

457   of Gm prepared using three separate "builds" of the *EcAMSat* fluidic system (different fluidic

458   cards, tubing sets, pumps, and valves) for dye concentrations corresponding to low, medium, and

459   high Gm levels. **B**) Optically measured exchange efficiency of *EcAMSat* fluidic wells after ~

460   400 μL of exchange fluid were pumped through each 100 μL well by the fluidic system for the

461   four banks of wells depicted in Figure 1; all wells contained stationary-phase *E. coli* in order to

462   include their impact on flow resistance through 0.2 μm pore-size filters at the inlet and outlet of

463   each well ($n = 12$ per condition per test). Error bars in both panels are ± one standard deviation.

464   **Figure 5. A**) Time-dependent changes during growth, antibiotic-treatment, and Alamar-

465   Blue-measurement phases of experiment using the *EcAMSat* optical system, fluidic card, and

466   fluidic delivery system. Curves show absorbance of oxidized (blue/turquoise curves) and

467   reduced (pink/magenta curves) forms of AB along with OD (turbidity; black/grey curves) due to

468   wild type ("WT") and mutant ("Mut") cells. **B**) Semi-log plot of OD due to cells (turbidity) from

469   the growth phase of Panel A for wild type (black) and mutant (green) strains, showing the

470   different growth phases. Error bars in both panels are ± one standard deviation.

471   **Figure 6. A**) Time dependence of absorbance due to oxidized (blue/turquoise) and

472   reduced (pink/magenta) forms of AB along with OD due to cells (turbidity; black/grey) for both

473   *E. coli* strains in absence of Gm. **B**) As in Panel A, but treated with Gm at 52 μg/mL. **C**)

474   Alamar Blue reduction curves (absorbance vs. time) for Gm = 0, 3.5, 14.6, and 52 μg/mL;

475   diagonal arrows start at control (Gm = 0), point through low and medium doses, and terminate at

476   highest dose. Line at $t = 11.5$ hour denotes point at which WT control has reduced 77% of

21

477   Alamar Blue, equivalent to the $t = 6$ hour data point of the conventional well-plate experiment

478   shown in Figure 3. **D**) Amount of Alamar Blue reduced in presence of 3.5, 14.6, and 52 µg/mL

479   Gm ("Low", "Medium", "High") normalized to the amount of AB reduced for the untreated

480   control for each strain at $t = 11.5$ hour of Panel C; $p < 0.0001$ for the high Gm dose. Error bars

481   for Panels A, B, and D are ± one standard deviation.

482

487

488   **CONTRIBUTIONS**

489   The study was originally conceived by ACM and built upon as work progressed by NASA/ARC

490   colleagues. The *EcAMSat* payload system, based on the previously flown PharmaSat spaceflight

491   payload,[13,14] was adapted in order to execute the experiments reported here. Changes in system

492   architecture and design were conceived by AJR, CCB, MPP, MC, and CRF. The biology

493   experiment was adapted for compatibility with the *EcAMSat* payload hardware by MPP, MPL,

494   and SC, who also conducted biology labwork at ARC with the participation of MRP and TNC.

495   The fluidics system, with integrated optical measurement capability, was modified, developed,

496   extensively tested and calibrated by MRP, TNC, MPL, MC, SSR, CMM, DTW, MXT, TDB, and

497   CCB. Software and mechanical engineering work on the *EcAMSat* payload was accomplished by

498   MC, CCB, AC, TVS, and CRF. AJR, MRP, and MPP developed and implemented data analysis

499   methods. MBH managed NASA engineering configuration and documentation and SMS is the

500 NASA *EcAMSat* project manager. J-HW and MK carried out experimental work at Stanford.

501 ACM, MRP, MPP, and AJR wrote the manuscript.

502

503 **REFERENCES**

504 1.   Hengge-Aronis R. Signal transduction and regulatory mechanisms involved in control of
505 the sigma(S) (*RpoS*) subunit of RNA polymerase. Microbiol Mol Biol Rev. 2002; **66**(3):373-395,
506 table of contents.
507 2.   Matin A. The molecular basis of carbon-starvation-induced general resistance in
508 *Escherichia coli*. Molecular microbiology. 1991; **5**(1):3-10.
509 3.   Matin A. Stress, Bacterial: General and Specific. In: Editor-in-Chief: Moselio S, editor.
510 Encyclopedia of Microbiology (Third Edition). Oxford: Academic Press; 2009. pp. 485-500.
511 4.   Matin AC. Stress, Bacterial: General and Specific. Reference Module in Biomedical
512 Sciences: Elsevier; 2014.
513 5.   Wang JH, Singh R, Benoit M, Keyhan M, Sylvester M, Hsieh M, *et al*. Sigma S-
514 dependent antioxidant defense protects stationary-phase *Escherichia coli* against the bactericidal
515 antibiotic gentamicin. Antimicrob Agents Chemother. 2014; **58**(10):5964-5975.
516 6.   Lynch SV, Brodie EL, Matin A. Role and regulation of sigma S in general resistance
517 conferred by low-shear simulated microgravity in *Escherichia coli*. J Bacteriol. 2004;
518 **186**(24):8207-8712.
519 7.   Lynch SV, Mukundakrishnan K, Benoit MR, Ayyaswamy PS, Matin A. *Escherichia coli*
520 biofilms formed under low-shear modeled microgravity in a ground-based system. Appl Environ
521 Microbiol. 2006; **72**(12):7701-7710.
522 8.   Singh R, Matin AC. Cellular Response of *Escherichia coli* to Microgravity and
523 Microgravity Analogue Culture. In: Nickerson AC, Pellis RN, Ott MC, editors. Effect of
524 Spaceflight and Spaceflight Analogue Culture on Human and Microbial Cells: Novel Insights
525 into Disease Mechanisms. New York, NY: Springer New York; 2016. pp. 259-282.
526 9.   Bascove M, Huin-Schohn C, Gueguinou N, Tschirhart E, Frippiat JP. Spaceflight-
527 associated changes in immunoglobulin VH gene expression in the amphibian *Pleurodeles waltl*.
528 FASEB J. 2009; **23**(5):1607-1615.
529 10.   Crucian BE, Stowe RP, Mehta SK, Yetman DL, Leal MJ, Quiriarte HD, *et al*. Immune
530 status, latent viral reactivation, and stress during long-duration head-down bed rest. Aviat Space
531 Environ Med. 2009; **80**(5 Suppl):A37-A44.
532 11.   Mehta SK, Stowe RP, Feiveson AH, Tyring SK, Pierson DL. Reactivation and shedding
533 of cytomegalovirus in astronauts during spaceflight. J Infect Dis. 2000; **182**(6):1761-1764.
534 12.   Nicholson WL, Ricco AJ, Agasid E, Beasley C, Diaz-Aguado M, Ehrenfreund P, *et al*.
535 The *O/OREOS* mission: first science data from the Space Environment Survivability of Living
536 Organisms (SESLO) payload. Astrobiology. 2011; **11**(10):951-958.
537 13.   Parra M, Ly D, Ricco AJ, McGinnis MR, Niesel D. The *PharmaSat* Nanosatellite
538 platform for life science experimentation: effects of spaceflight on antifungal activity against
539 *Saccharomyces cerevisiae*. Gravitational and Space Biology. 2009; **23**(30):30.
540 14.   Ricco AJ, Parra M, Niesel D, Piccini M, Ly D, McGinnis M, *et al*. *PharmaSat*: drug dose
541 response in microgravity from a free-flying integrated biofluidic/optical culture-and-analysis

542 satellite. Proc. SPIE 7929, Microfluidics, BioMEMS, and Medical Microsystems IX. SPIE:
543 Bellingham, WA, 2011:79290T (9 pp).
544 15.　Woellert K, Ehrenfreund P, Ricco AJ, Hertzfeld H. Cubesats: Cost-effective science and
545 technology platforms for emerging and developing nations. Advances in Space Research. 2011;
546 **47**(4):663-684.
547 16.　Zgurskaya HI, Keyhan M, Matin A. The sigma S level in starving *Escherichia coli* cells
548 increases solely as a result of its increased stability, despite decreased synthesis. Mol Microbiol.
549 1997; **24**(3):643-651.
550 17.　Kolter R, Siegele DA, Tormo A. The stationary phase of the bacterial life cycle. Annu
551 Rev Microbiol. 1993; **47**:855-874.
552 18.　Sonenshein AL. CodY, a global regulator of stationary phase and virulence in Gram-
553 positive bacteria. Curr Opin Microbiol. 2005; **8**(2):203-207.
554 19.　Llorens JM, Tormo A, Martínez-García E. Stationary phase in gram-negative bacteria.
555 FEMS Microbiol Rev. 2010; **34**(4):476-495.
556 20.　Cabeen MT. Stationary phase-specific virulence factor overproduction by a lasR mutant
557 of *Pseudomonas aeruginosa*. PLoS One. 2014; **9**(2):e88743.
558 21.　Mouslim C, Hughes KT. The effect of cell growth phase on the regulatory cross-talk
559 between flagellar and Spi1 virulence gene expression. PLoS Pathog. 2014; **10**(3):e1003987.
560 22.　Dalebroux ZD, Svensson SL, Gaynor EC, Swanson MS. ppGpp conjures bacterial
561 virulence. Microbiol Mol Biol Rev. 2010; **74**(2):171-199.
562 23.　Roop II RM, Gee JM, Robertson GT, Richardson JM, Ng WL, Winkler ME. *Brucella*
563 stationary-phase gene expression and virulence. Annu Rev Microbiol. 2003; **57**:57-76.
564 24.　Mangan MW, Lucchini S, Danino V, Croinin TO, Hinton JC, Dorman CJ. The
565 integration host factor (IHF) integrates stationary-phase and virulence gene expression in
566 *Salmonella enterica serovar Typhimurium*. Molecular microbiology. 2006; **59**(6):1831-1847.
567 25.　Kau AL, Hunstad DA, Hultgren SJ. Interaction of uropathogenic *Escherichia coli* with
568 host uroepithelium. Curr Opin Microbiol. 2005; **8**(1):54-59.
569 26.　Kau AL, Martin SM, Lyon W, Hayes E, Caparon MG, Hultgren SJ. *Enterococcus*
570 *faecalis* tropism for the kidneys in the urinary tract of C57BL/6J mice. Infect Immun. 2005;
571 **73**(4):2461-2468.
572 27.　Matin A, Auger EA, Blum PH, Schultz JE. Genetic basis of starvation survival in
573 nondifferentiating bacteria. Annu Rev Microbiol. 1989; **43**:293-316.
574 28.　Yi B, Crucian B, Tauber S, Ullrich O, Choukèr A. Immune Dysfunction in Spaceflight:
575 An Integrative View. In: Nickerson AC, Pellis RN, Ott MC, editors. Effect of Spaceflight and
576 Spaceflight Analogue Culture on Human and Microbial Cells: Novel Insights into Disease
577 Mechanisms. New York, NY: Springer New York; 2016. pp. 61-79.
578 29.　Barrila J, Wilson JW, Soni A, Yang J, Mark Ott C, Nickerson CA. Using Spaceflight and
579 Spaceflight Analogue Culture for Novel Mechanistic Insight into *Salmonella* Pathogenesis. In:
580 Nickerson AC, Pellis RN, Ott MC, editors. Effect of Spaceflight and Spaceflight Analogue
581 Culture on Human and Microbial Cells: Novel Insights into Disease Mechanisms. New York,
582 NY: Springer New York; 2016. pp. 209-235.
583 30.　Gueguinou N, Huin-Schohn C, Bascove M, Bueb JL, Tschirhart E, Legrand-Frossi C, *et*
584 *al*. Could spaceflight-associated immune system weakening preclude the expansion of human
585 presence beyond Earth's orbit? J Leukoc Biol. 2009; **86**(5):1027-1038.
586 31.　Stowe RP, Sams CF, Pierson DL. Adrenocortical and immune responses following short-
587 and long-duration spaceflight. Aviat Space Environ Med. 2011; **82**(6):627-634.

588   32.   Stowe RP, Kozlova EV, Sams CF, Pierson DL, Walling DM. Latent and lytic Epstein-
589   Barr virus gene expression in the peripheral blood of astronauts. J Med Virol. 2011; **83**(6):1071-
590   1077.
591   33.   Wilson JW, Ott CM, Honer zu Bentrup K, Ramamurthy R, Quick L, Porwollik S, *et al*.
592   Space flight alters bacterial gene expression and virulence and reveals a role for global regulator
593   Hfq. Proc Natl Acad Sci U S A. 2007; **104**(41):16299-16304.
594   34.   Tixador R, Richoilley G, Gasset G, Planel H, Moatti N, Lapchine L, *et al*. Preliminary
595   results of Cytos 2 experiment. Acta Astronaut. 1985; **12**(2):131-134.
596   35.   Juergensmeyer MA, Juergensmeyer EA, Guikema JA. Long-term exposure to spaceflight
597   conditions affects bacterial response to antibiotics. Microgravity Sci Technol. 1999; **12**(1):41-47.
598   36.   Klaus D, Simske S, Todd P, Stodieck L. Investigation of space flight effects on
599   *Escherichia coli* and a proposed model of underlying physical mechanisms. Microbiology. 1997;
600   **143** (Pt 2):449-455.
601   37.   Kacena MA, Merrell GA, Manfredi B, Smith EE, Klaus DM, Todd P. Bacterial growth in
602   space flight: logistic growth curve parameters for *Escherichia coli* and *Bacillus subtilis*. Appl
603   Microbiol Biotechnol. 1999; **51**(2):229-234.
604   38.   Vukanti R, Model MA, Leff LG. Effect of modeled reduced gravity conditions on
605   bacterial morphology and physiology. BMC Microbiol. 2012; **12**:4.
606   39.   Zhang Y, Lai C, Duan J, Guan N, Ullah K, Deng Y. Simulated microgravity affects
607   semicarbazide-sensitive amine oxidase expression in recombinant *Escherichia coli* by HPLC-
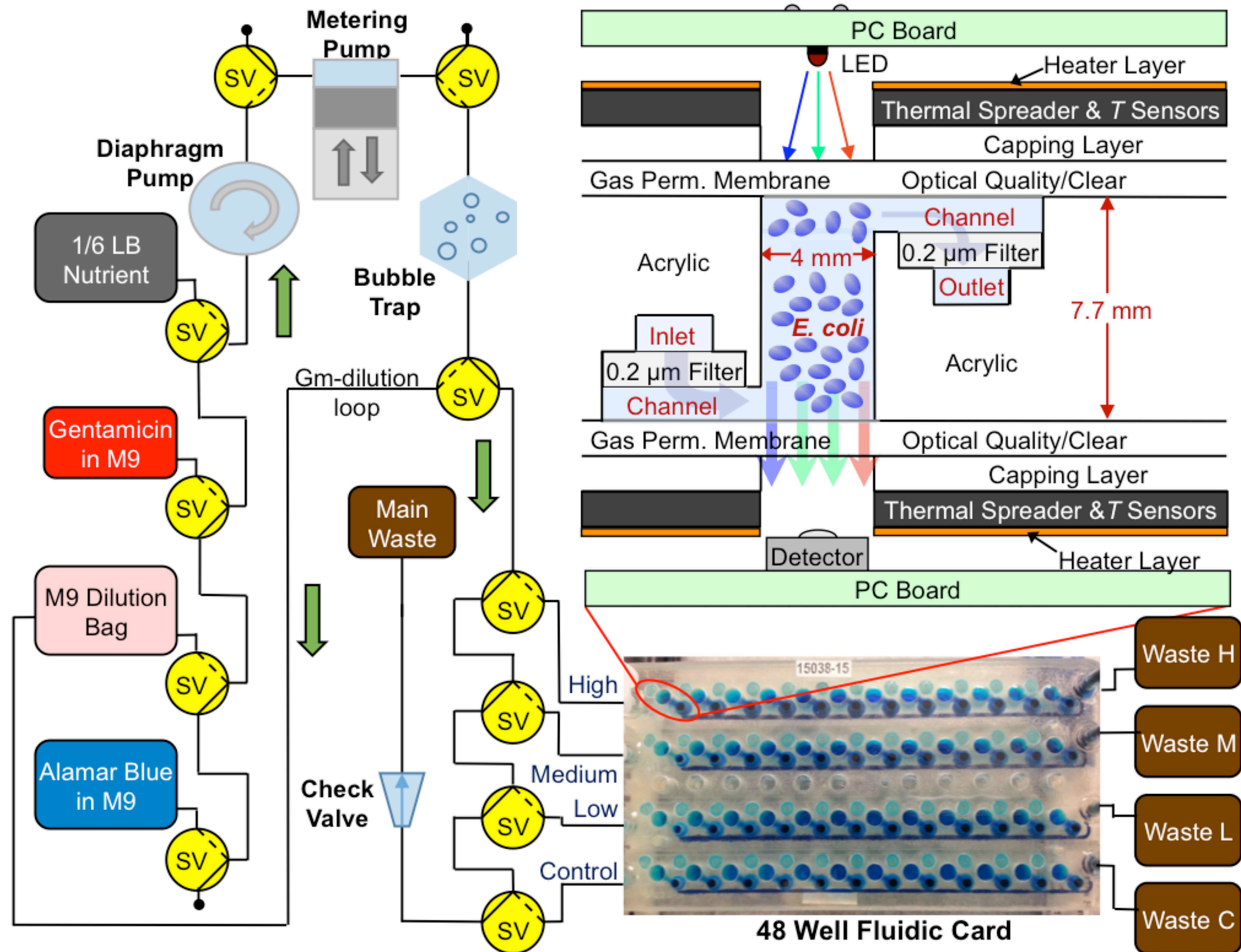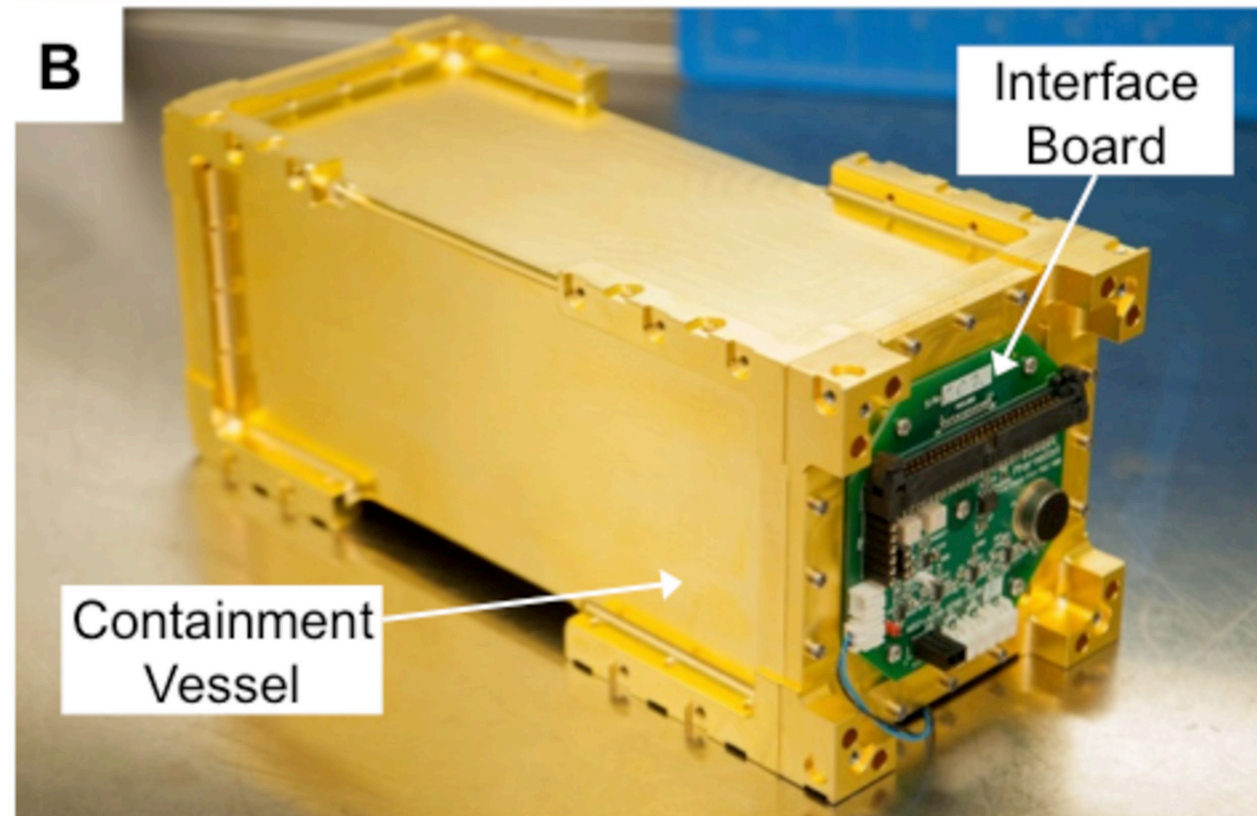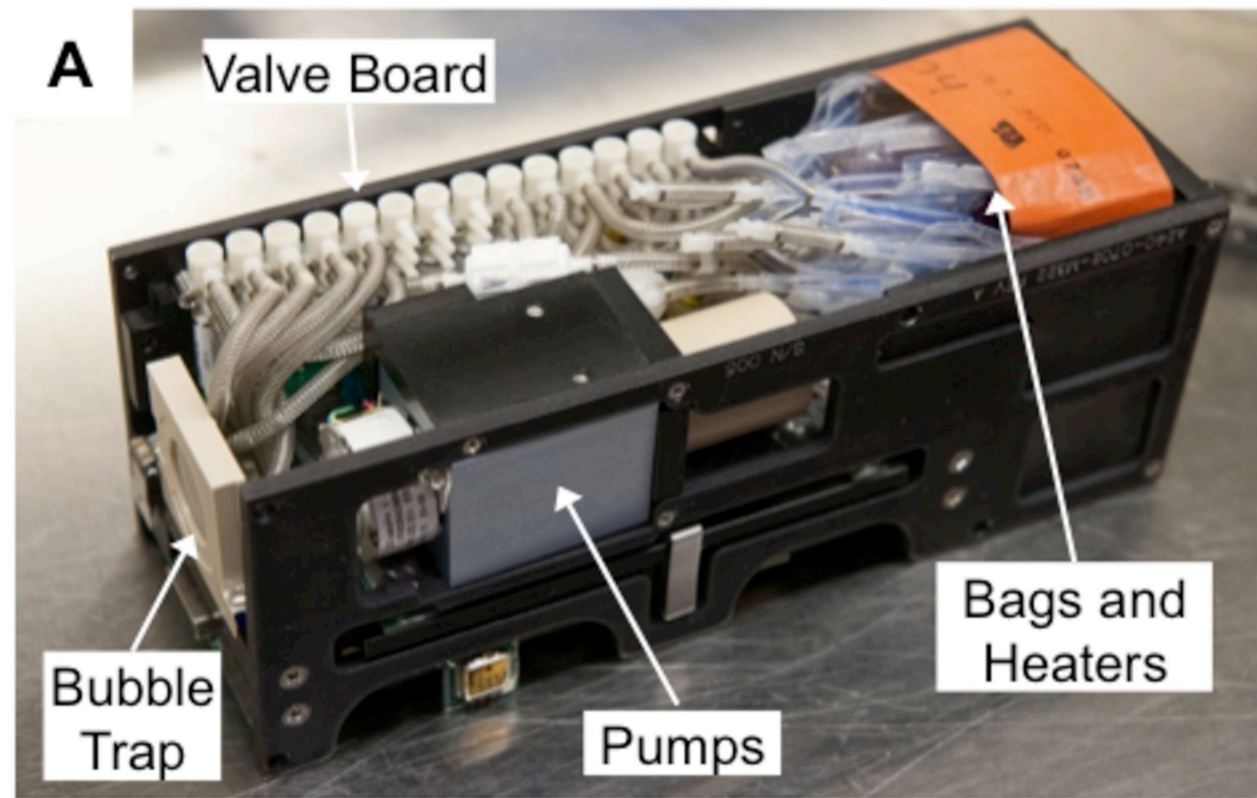608   ESI-QQQ analysis. Appl Microbiol Biotechnol. 2012; **94**(3):809-816.

48 Well Fluidic Card

Figure 1

A
Valve Board
Bubble Trap
Pumps
Bags and Heaters

B
Interface Board
Containment Vessel

C

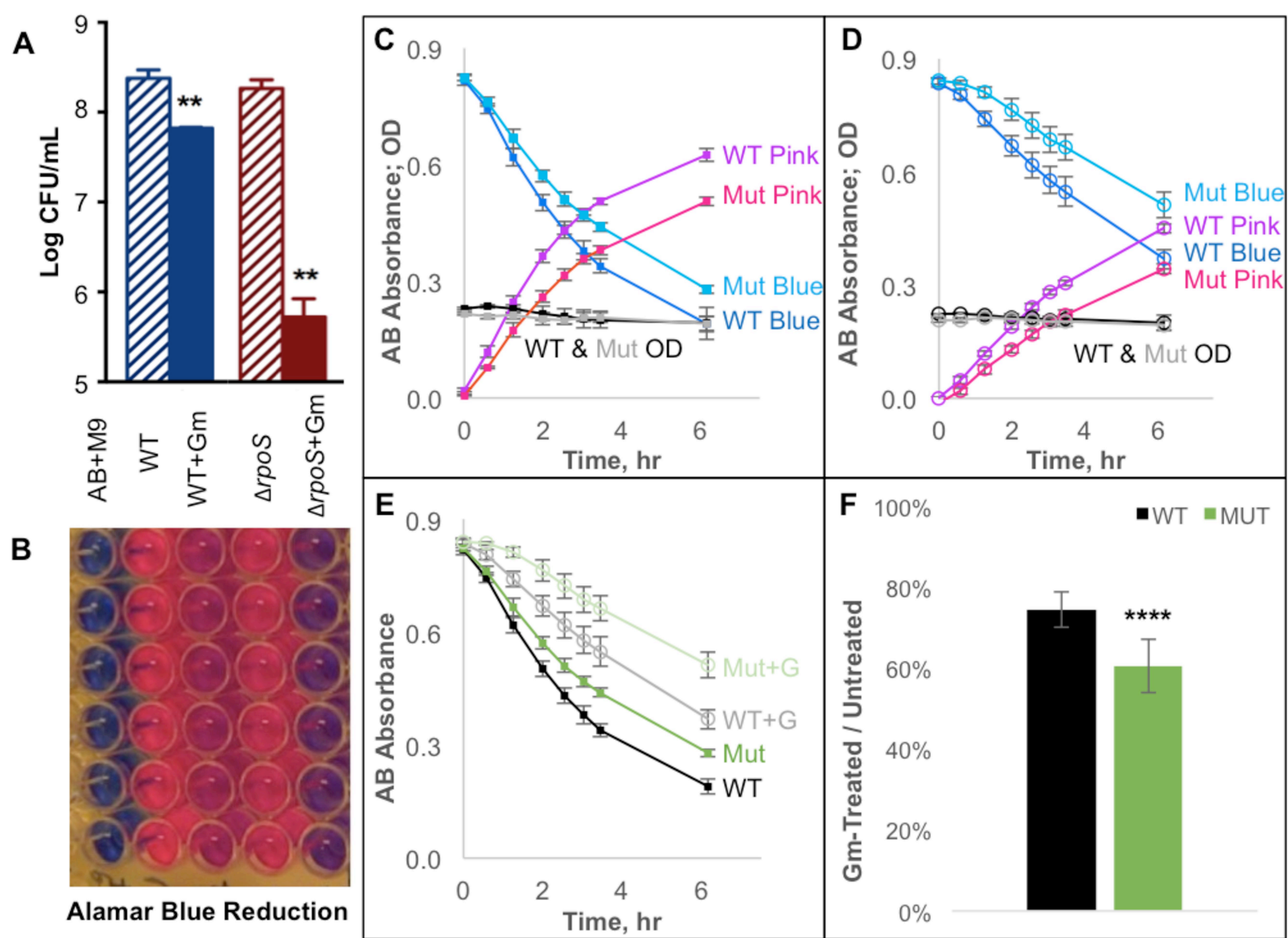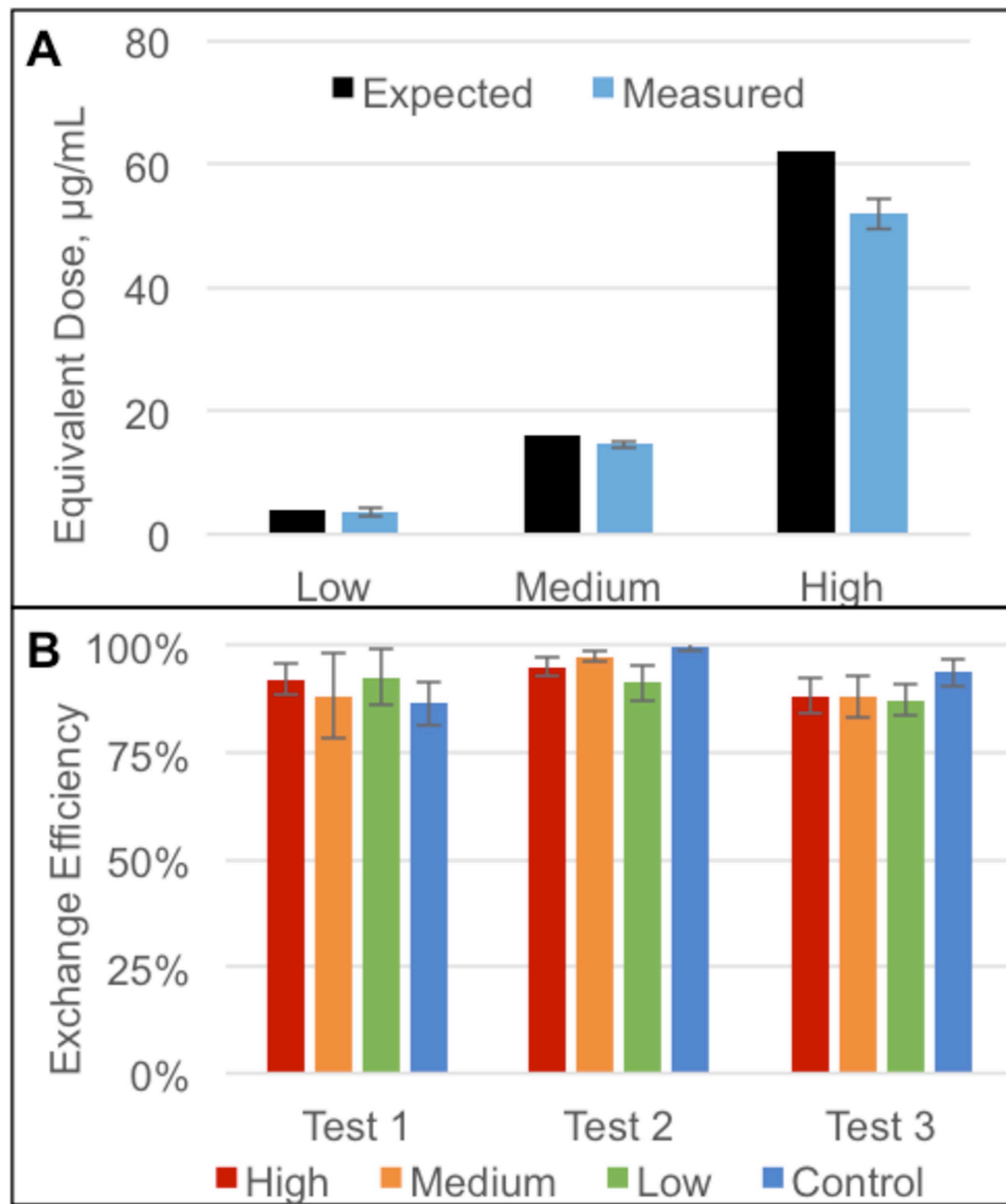| Growth 48 hr	Challenge 48 hr	Measure 56 hr
Pumping	Pumping	Pumping
Growth to Stationary w/ 1/6 LB	Antibiotic Incubation	Alamar Blue Viability Measurements

Temp control ON: Incubate at 37°C

Optics ON: 15 min Readings

Figure 2

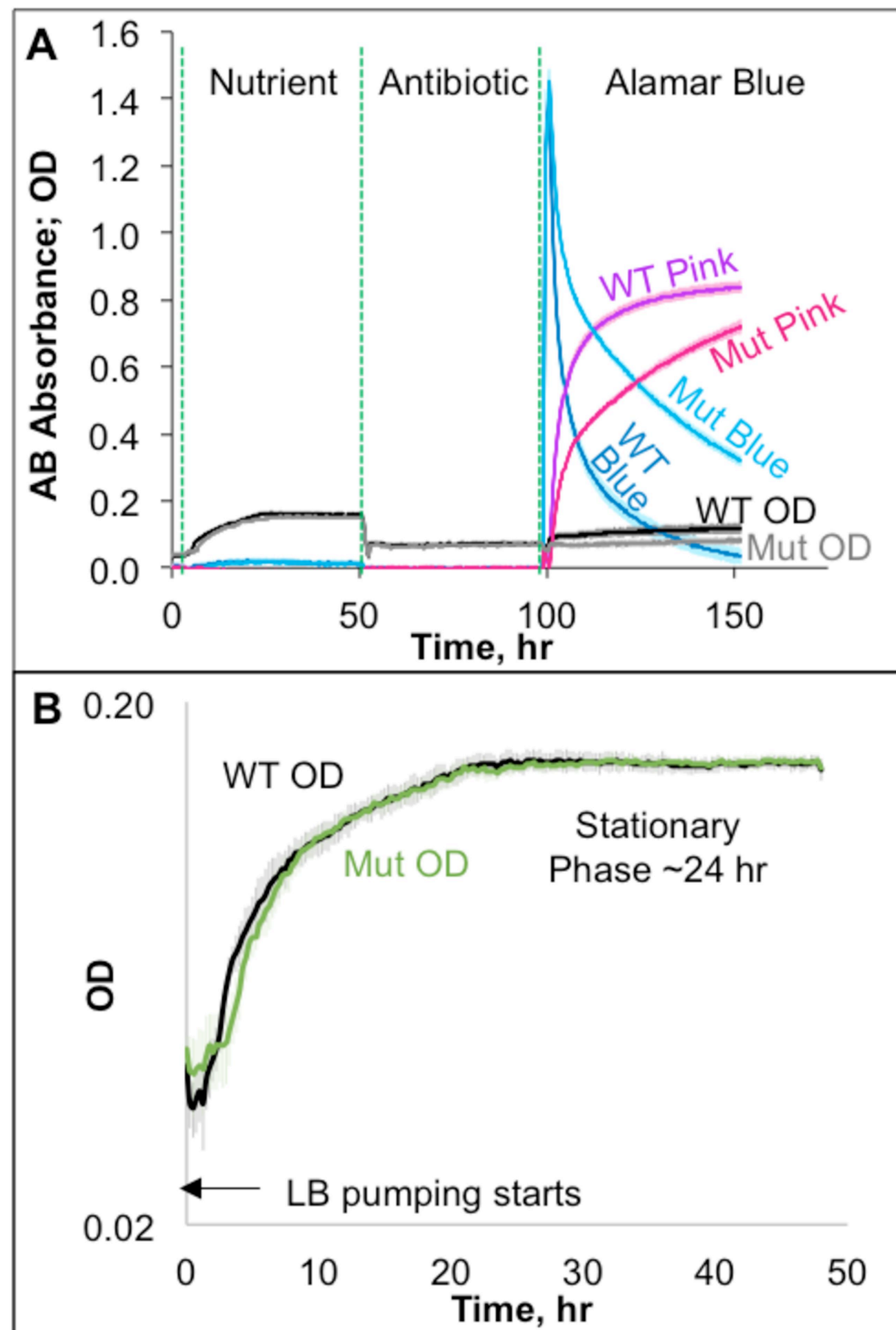**Alamar Blue Reduction**

Figure 3

Figure 4

Figure 5

Figure 6